NEW ADDITIVE WATERMARK DETECTORS BASED ON A HIERARCHICAL SPATIALLY ADAPTIVE IMAGE MODEL

by

Antonis Mairgiotis[1], Nikolaos Galatsanos[1,*] , and Yongi Yang[2]

[1]Department of Computer Science
University of Ioannina
Ioannina, Greece 45110
{*mairgiot, galatsanos@cs.uoi.gr*}

[2]Department of Electrical and Computer Engineering
Illinois Institute of Technology
Chicago, IL 60616, USA
{*yy@ece.iit.edu*}

ABSTRACT

In this paper we propose a new family of watermark detectors for additive watermarks in digital images. These detectors are based on a recently proposed two-level, hierarchical image model, which was found to be beneficial for image recovery problems. The top level of this model is defined to exploit the spatially-varying local statistics of the image, while the bottom level is used to characterize the image variations along two principal directions. Based on this model we derive a class of detectors for the additive watermark detection problem, including a detector similar in spirit to a generalized likelihood ratio test (GLRT), Bayesian, and Rao test detectors. We also propose methods to estimate the necessary parameters for these detectors. Our numerical experiments demonstrate that these new detectors can lead to superior performance to several state-of-the-art detectors.

* Corresponding author

1. INTRODUCTION

Additive watermark detection can be formulated as a hypothesis testing problem, where one needs to determine the presence or absence of a known watermark in an image. Within such a formulation, the watermark is treated as the known signal and the image is treated as the corrupting noise [1] and [2]. To derive a test statistic for this problem, such as the likelihood ratio test detector, a statistical model for the image has to be defined.

A well known and widely used detector for watermarking is the correlation detector. It is straightforward to show that this detector can be derived using the likelihood ratio test criterion under the assumption that that image pixels are independent, identically distributed (IID) Gaussian random variables [1]. While such an image model greatly simplifies the problem, it is often not accurate in characterizing the image properties. Alternatively, detectors are proposed based on the use of a high-pass filter to "pre-whiten" the image before the correlation detector is applied [1]. In such detectors the output of the high-pass filter rather than the image is modeled by IID Gaussian random variables. While an improvement over its predecessor, this model is found to be sometimes inadequate for characterizing the residuals of the image (i.e., the output of the high-pass filter). For example, in the vicinity of edges in the image large residual values will be produced by the high-pass filter, which will lead to heavy tails in the observed residual statistics [9].

In recent years there have been considerable efforts in the research community in the development of image models for improved watermark detection. In [3] Hernandez *et al* proposed an optimal detector for watermarking based on the assumption of a generalized Gaussian density (GGD) function for the discrete cosine transform (DCT) coefficients of the image. In [4] a Weibull distribution was used for the discrete Fourier transform (DFT) coefficients of the image. In [5] and [6] optimal detectors were derived for both additive and multiplicative watermarking by assuming GGD distributions for the DCT, DFT, and discrete wavelet transform (DWT) coefficients of the image. In [7] Nikolaidis and Pitas proposed

asymptotically optimal detectors by using GGD models for the DCT and DWT coefficients. In [8] Briassouli *et al* used α -stable distributions for the DCT coefficients of the image.

In this paper we propose the use of a hierarchical, locally adaptive image model for watermark detection. The top level of this model is defined to exploit the spatially-varying local statistics of the image. This model can be viewed as a generalization of the concept of line process used in the context of compound Markov random fields [23] and [24]. The difference is that a continuous model, rather than binary edges, is used for characterizing the local discontinuities in the image. Using this image model we will derive several detectors for additive watermarking, including a "pseudo generalized likelihood ratio test" (*PGLRT*), Bayesian, and the Rao test detectors. The term "pseudo" is used since we use maximum a posteriori and not maximum likelihood (ML) estimates for the unknown parameters as the generalized likelihood ratio test requires [28].

We note that this hierarchical image model used in this study was recently developed for image restoration in [22]. It is interesting to note that the development of image models has also been very important for the classical image denoising and restoration problems, in which a statistical image model is essential [9] for various estimation methodologies, e.g., maximum a posteriori estimation. For example, the simultaneous autoregressive (SAR) image prior has been used extensively in image restoration, e.g., [10]-[14]; "edge preserving" image priors are based either on modeling the residuals of the image or on a decorrelating transform (e.g., wavelet), e.g., [15]-[20].

The rest of this paper is organized as follows. In Section 2 we introduce the hierarchical image model and formulate its use for additive watermark detection. In Section 3 the *PGLRT* detector is derived and methods to estimate the necessary parameters of the model are given. Bayesian and Rao test based detectors are derived in Section 4. In Section 5 numerical results are given to demonstrate the proposed detectors. Conclusions are drawn in Section 6. For completeness, in the Appendix we provide the details on the detectors used for comparison in our experiments, which were based on wavelet transform and GGD modeling.

2. IMAGE MODEL AND ADDITIVE WATERMARKING

The image model we propose to use in this paper is based on the first order differences of the image along the two principal directions. Specifically, consider an image $\mathbf{f}$, whose pixels are denoted by $f(i,j)$. At pixel location (i,j), we define the image directional differences (IDD) along the horizontal and vertical directions, respectively, as follows:

$$\varepsilon_1(i,j) = f(i,j) - f(i,j+1), \quad \varepsilon_2(i,j) = f(i,j) - f(i+1,j). \tag{1}$$

We assume that these IDDs obey a Gaussian probability density function (pdf), given by

$$\varepsilon_k(i,j) \sim N\left(0, a_k^{-1}(i,j)\right), \tag{2}$$

where $a_k^{-1}(i,j)$ is the variance parameter.

For notational convenience, in the rest of the paper we will denote the IDDs using a single index as $\boldsymbol{\varepsilon}_k = \left[\varepsilon_k(1), \varepsilon_k(2), ..., \varepsilon_k(N)\right]^T$, k=1,2, where N is the total number of image pixels. In addition, let $\tilde{\boldsymbol{\varepsilon}} = \left[\boldsymbol{\varepsilon}_1^T, \boldsymbol{\varepsilon}_2^T\right]^T$, a vector consisting of IDDs in both directions.

Assuming independence of the IDDs, we can write the joint pdf

$$p(\tilde{\boldsymbol{\varepsilon}}; \tilde{\mathbf{a}}) \propto \prod_{k=1}^{2} \prod_{i=1}^{N} \left[a_k^{1/2}(i) \exp\left(-\frac{1}{2} a_k(i) \left(\varepsilon_k(i)\right)^2 \right) \right], \tag{3}$$

where $\tilde{\mathbf{a}} = \left[\mathbf{a}_1^T, \mathbf{a}_2^T\right]^T$, $\mathbf{a}_k = \left[a_k(1), a_k(2), ..., a_k(N)\right]^T$, $k = 1, 2$ which denotes the corresponding variance parameters. In this form index i denotes a pixel location in lexicographic order.

The pdf in (3) allows the flexibility that the local variance can vary from pixel to pixel. This is desirable for modeling the spatially non-stationary properties of the image (e.g., edges). Unfortunately, it includes as many variance parameters $a_k(i)$ as the number of image pixels. To avoid the problem of over-fitting, it is necessary to impose additional constraint on

the model to limit its degrees of freedom. For this purpose we model $a_k(i)$ as random variables, and define a hyper-prior on them.

In this work we use a Gamma pdf for the hyper-prior [27], which is of the form

$$p(a_k(i);m,l) \propto a_k^{\frac{l-2}{2}}(i)\ \exp\{-m(l-2)a_k(i)\},\ k=1,2, \tag{4}$$

where *m* and *l* are the parameters of the Gamma distribution. Such a choice is motivated by the fact that the Gaussian and the Gamma families are conjugate [26] with respect to the inverse of the variance of the Gaussian, of which the benefit will become clear later in the estimate of the model parameters. This combination has also been used successfully in sparse Bayesian models for machine learning tasks [25].

For the Gamma pdf in (4), we have

$$E\left[a_k(i)\right] = l\left(2m\left(l-2\right)\right)^{-1}, \text{ and } Var\left[a_k(i)\right] = l\left(2m^2\left(l-2\right)^2\right)^{-1}.$$

Assuming that $a_k(i)$ are independent and identically distributed, then we have

$$p(\tilde{\mathbf{a}};m,l) = C\cdot\prod_{k=1}^{2}\prod_{i=1}^{N}\left(a_k^{\frac{l-2}{2}}(i)\ \exp\{-m(l-2)a_k(i)\}\right), \tag{5}$$

where C is a normalization constant.

To illustrate the properties of the proposed image model, we show an example in Figures 4 the estimated values of $a_k^{-1}(i), k=1,2$ from the "Lena" image in Figure 1 (of which the detail of the estimate will be provided in Sect. 5). It can be seen that the parameters $a_k^{-1}(i)$ can effectively capture the spatially-varying local statistics of the image. Notably, the edge structures along respective directions in the image have been highlighted by the large values of $a_k^{-1}(i)$. In this regard, the parameters $a_k^{-1}(i)$ can be viewed as a generalization of the line process used in the context of compound Markov random fields (CMRF) [23] and [24]. More specifically, in the case of CMRFs the square of the difference between two adjacent pixel is either used or omitted from the prior depending on the value of the binary line process between these pixels. When the line process has value 1 they are omitted when the line process has value 0 they are included. For our model all differences are included in

the prior. However, they are weighted according to strength of the edge that lies between them. In the vicinity of edges this weight is small while in smooth areas it is large. Thus, our model does not "quantize" image discontinuities.

This two level model since in essence models the pdfs of the IDDs as an infinite mixture of Gaussians with zero mean and different variances which is very flexible and captures very accurately the IDDs statistics. Looking at this model from another point of view one can observe that if we marginalize the inverse variances of this two level model the resulting pdfs of the IDDs become Student-t [25]. This pdf is very flexible and can have heavy tails which is very useful for robust modeling. Furthermore, it can behave, depending on the values of its parameters, from a Gaussian to a uniform [31]. Such models provide a very elegant mechanism that allows us to describe in detail the local image structure. This is very useful in many low level image processing applications such as image recovery [22], [32]-[34] and image watermarking as we demonstrate herein.

In the additive watermark detection problem one has to decide between the following two hypotheses

$$\begin{aligned} H_0 &: \mathbf{y} = \mathbf{f} \\ H_1 &: \mathbf{y} = \mathbf{f} + \gamma \mathbf{w} \end{aligned} \tag{6}$$

where $\mathbf{y}$ and $\mathbf{f}$ are the observed and the original images, respectively, and $\mathbf{w}$ is the watermark signal and γ is its strength.

The image directional difference operators, $\mathbf{Q}_k$, $k=1,2$ are defined by $\mathbf{Q}_k\mathbf{f} = \boldsymbol{\varepsilon}_k$ using the $\boldsymbol{\varepsilon}_k$ in Eq. (1). Applying the directional difference operators $\mathbf{Q}_k$, $k=1,2$, to the observed image in (6), we obtain

$$\begin{aligned} H_0 &: \mathbf{y}_k^{'} = \boldsymbol{\varepsilon}_k \\ H_1 &: \mathbf{y}_k^{'} = \boldsymbol{\varepsilon}_k + \gamma \mathbf{w}_k^{\prime} = \boldsymbol{\varepsilon}_k + \mathbf{w}_k^{\prime\prime} \end{aligned} \tag{7}$$

where $\mathbf{y}_k^{'} = \mathbf{Q}_k\mathbf{y}$, $\boldsymbol{\varepsilon}_k = \mathbf{Q}_k\mathbf{f}$, $\mathbf{w}_k^{\prime\prime} = \gamma\mathbf{Q}_k\mathbf{w}$, $k=1,2$.

Based on Eqs. (3) and (5), the conditional pdfs of the observations for the two hypotheses in Eq. (7) can be written as

$$p(\tilde{\mathbf{y}}';\tilde{\mathbf{a}},H_0)=C\cdot\left\{\prod_{k=1}^{2}\prod_{i=1}^{N}a_k(i)^{1/2}\right\}\exp\left(-\frac{1}{2}\sum_{k=1}^{2}\sum_{i=1}^{N}a_k(i)\left(y_k'(i)\right)^2\right)$$
$$p(\tilde{\mathbf{y}}';\tilde{\mathbf{a}},H_1)=C\cdot\left\{\prod_{k=1}^{2}\prod_{i=1}^{N}a_k(i)^{1/2}\right\}\exp\left(-\frac{1}{2}\sum_{k=1}^{2}\sum_{i=1}^{N}a_k(i)\left(y_k'(i)-w_k''(i)\right)^2\right) \quad (8)$$

where $\tilde{\mathbf{y}}'=\left[\mathbf{y}_1'^{T},\mathbf{y}_2'^{T}\right]^T$. In what follows these pdfs will be used to derive the *PGLRT*, Bayesian, and Rao test detectors.

3. PSEUDO GENERALIZED LIKELIHOOD RATIO DETECTOR

The likelihood ratio test for the hypothesis testing problem in Eq. (7) is given by

$$LRT(\tilde{\mathbf{y}}';\tilde{\mathbf{a}})=\log\left\{\frac{p(\tilde{\mathbf{y}}';\tilde{\mathbf{a}},H_1)}{p(\tilde{\mathbf{y}}';\tilde{\mathbf{a}},H_0)}\right\}\underset{\mathrm{H_0}}{\overset{\mathrm{H_1}}{\gtrless}}0\,. \quad (9)$$

Unfortunately, the parameters $\tilde{\mathbf{a}}$ are not known, and the test in (9) cannot be used directly. In such a case the generalized likelihood ratio test (GLRT) is usually employed, where one uses *estimates* of the unknown parameters [28]. The GLRT is given by

$$GLRT(\tilde{\mathbf{y}}')=\log\left\{\frac{p(\tilde{\mathbf{y}}';\hat{\tilde{\mathbf{a}}}_{/H_1},H_1)}{p(\tilde{\mathbf{y}}';\hat{\tilde{\mathbf{a}}}_{/H_0},H_0)}\right\}\underset{\mathrm{H_0}}{\overset{\mathrm{H_1}}{\gtrless}}0\,, \quad (10)$$

where $\hat{\tilde{\mathbf{a}}}_{/H_0}$, $\hat{\tilde{\mathbf{a}}}_{/H_1}$ are the ML estimates of $\tilde{\mathbf{a}}$ in Eq. (9) under the two hypotheses. In what follows since we do not use the ML estimates in Eq. (10) we term our detectors as "pseudo GLRT" (*PGLRT*).

With the conditional pdfs in Eq. (8), the test statistic for the detector in Eq. (10) can be written as

$$T\left(\tilde{\mathbf{y}}'\right)=\sum_{k=1}^{2}\sum_{i=1}^{N}y_k'(i)^2\left(\hat{a}_k(i)_{/H_0}-\hat{a}_k(i)_{/H_1}\right)-\hat{a}_k(i)_{/H_1}w_k''(i)^2-2y_k'(i)w_k''(i)\hat{a}_k(i)_{/H_1}\,. \quad (11)$$

For weak watermarks, it is reasonable to expect that the estimates $\hat{a}_k(i)_{/H_0},\hat{a}_k(i)_{/H_1}$ are approximately equal. Thus, the test statistic in Eq. (11) can be simplified as (upon ignoring the middle term as it does not depend directly on the data)

$$T_{PGLRT}\left(\tilde{\mathbf{y}}'\right)=\sum_{k=1}^{2}\sum_{i=1}^{N}y'_k(i)w''_k(i)\hat{a}_k(i)_{/H_1}\underset{H_0}{\overset{H_1}{\gtrless}}T\,, \tag{12}$$

where T is a threshold that determines the false alarm vs. probability of detection tradeoff of the detector [28].

The simplified test statistic in (12) offers a rather informative insight on the *PGLRT* detector. It assumes essentially the form of a matched filter, where the observation at each pixel is normalized by its local variance.

The test statistic in (11) and (12) requires the estimates of the parameters $\hat{a}_k(i)$. Obviously, the ML estimate here will be problematic because only one data point is available. Instead, we use a maximum a posteriori estimate instead, where the hyper-prior $p(\tilde{\mathbf{a}};m,l)$ is used to ameliorate this difficulty. By invoking the Bayes' law, this estimate is obtained as

$$\hat{a}_k\left(i\right)_{/H_0}=\arg\max_{a_k(i)}\left\{\log p\left(\tilde{\mathbf{a}}\,|\,\tilde{\mathbf{y}}',H_0,m,l\right)\right\}=\arg\max_{a_k(i)}\left\{\log p\left(\tilde{\mathbf{y}}'\,|\,\tilde{\mathbf{a}},H_0\right)+\log p\left(\tilde{\mathbf{a}};m,l\right)\right\},$$

and similarly for $\hat{a}_k\left(i\right)_{/H_1}$. After some algebra, it can be shown that

$$\hat{a}_k\left(i\right)_{/H_0}=\frac{1+(l-2)}{(y'_k(i))^2+2m(l-2)},\ \text{and}\ \hat{a}_k\left(i\right)_{/H_1}=\frac{1+(l-2)}{(y'_k(i)-w''_k(i))^2+2m(l-2)}\,. \tag{13}$$

It is interesting to examine the effect of the parameter l in this estimate. As $l\to\infty$ the estimate becomes $\hat{a}_k\left(i\right)=\left(2m\right)^{-1}$ for both H_0 and H_1. That is, the prior dominates the estimate. On the other hand, as $l\to 2$, the prior parameters disappear in (13), and the estimate simply degenerates to the ML estimate. For $l\in\left(2,\infty\right)$, the prior "regularizes" the estimate $\hat{a}_k\left(i\right)$ where the ML estimate is unstable because of lack of data.

In our experiments we tested both the *PGLRT* detector in Eq. (11) and its approximate in (12), and found that their performance was almost identical. For this purpose in the rest of this paper we will report results with the simplified one in Eq. (12).

At this point it is worth pointing out that the test statistic of the proposed *PGLRT* detector in Eq. (12) follows a Gaussian pdf under both hypotheses. The test statistic under hypothesis H_1 has mean value and variance

$E\left(T_{GLRT};H_1\right)=\sum_{k=1}^{2}\sum_{i=1}^{N}a_k\left(i\right)w_k''(i)^2$, $Var\left(T_{PGLRT};H_1\right)=\sum_{k=1}^{2}\sum_{i=1}^{N}a_k\left(i\right)w_k''(i)^2$

respectively. Similarly, the test statistic distribution under hypothesis H_0 has mean value $E(T_{PGLRT};H_0)=0$ and variance $Var\left(T_{PGLRT};H_0\right)=\sum_{k=1}^{2}\sum_{i=1}^{N}a_k\left(i\right)w_k''(i)^2$. Thus, the derivation of probability of false alarm and probability of detection is then straight forward [28].

4. BAYESIAN AND RAO DETECTORS

An alternative strategy to deal with the unknown parameters $\tilde{\mathbf{a}}$ in the LRT detector in Eq. (9) is to "marginalize" them using the hyper-prior [28]. This leads to the Bayesian detector given by

$$\mathrm{B}(\bar{\mathbf{y}}';m,l)=\log\left\{\frac{\int p\left(\tilde{\mathbf{y}}'\mid\tilde{\mathbf{a}},H_1\right)p\left(\tilde{\mathbf{a}};m,l\right)d\tilde{\mathbf{a}}}{\int p\left(\tilde{\mathbf{y}}'\mid\tilde{\mathbf{a}},H_0\right)p\left(\tilde{\mathbf{a}};m,l\right)d\tilde{\mathbf{a}}}\right\}\begin{matrix}H_1\\>\\<\\H_0\end{matrix}0\,. \tag{14}$$

It is important to note that the integration terms in Eq. (14) can be computed in closed form. This is guaranteed by the choice of the Gamma pdf as hyper-prior which is conjugate with the Gaussian [26], because the integrals in Eq. (14) are Gamma integrals of the form $\int x^{a-1}e^{-x\beta}=\Gamma(a)\beta^a$. Indeed, after some algebra and upon absorbing into the threshold T the terms in Eq. (14) that do not depend on the observations, one can show that the test statistic for Bayesian detector is given by

$$T_B\left(\tilde{\mathbf{y}}';m,l\right)=\sum_{k=1}^{2}\sum_{i=1}^{N}\log\left(\frac{(y_k'(i)-w_k''(i))^2+2m(l-2)}{(y_k'(i))^2+2m(l-2)}\right)\begin{matrix}H_1\\>\\<\\H_0\end{matrix}T\,. \tag{15}$$

By comparing the detector above with the *PGLRT* in Eq. (12), we can observe that in the Bayesian detector the influence of the variance parameters $a_k(i)$ of the image model is now exhibited in the form of the parameters of the hyper-prior.

Interestingly, recall the Bayesian estimate for the variance parameters earlier in Eq. (13). One can rewrite Bayesian detector in Eq. (15) as

$$T_B\left(\tilde{\mathbf{y}}';m,l\right)=\sum_{k=1}^{2}\sum_{i=1}^{N}\log\frac{\hat{a}_k\left(i\right)_{/H_0}}{\hat{a}_k\left(i\right)_{/H_1}} \underset{H_0}{\overset{H_1}{\gtrless}} T\,. \tag{16}$$

The form above provides an intuitive insight on the Bayesian detector. The test statistic is formed by comparing the variance of the IDDs at individual pixels. The presence of a watermark signal will increase the value of the variance estimate under H_1, thereby leading to a smaller value of the test statistic.

Thus far in deriving the watermark detectors we have considered the situations that the watermark strength is exactly known (i.e., parameter γ in Eq. (6)). There are also situations it might not be known, e.g., in public watermarking. In such a case one could treat γ the same way as other model parameters and use its estimate in the *PGLRT* detector. However, this becomes problematic in applications where the watermark signal is much weaker than the cover image. Our experiments indicate that this can greatly compromise the accuracy of the ML estimate of γ. In order to address this difficulty, we use the Rao test, which is a locally optimal detector (LOD) with performance close to that of a clairvoyant *PGLRT* (when γ is small) [29]. This detector was first introduced to the image watermarking problem in [7].

The Rao test for the observations in Eq. (7) is given by

$$T_R\left(\tilde{\mathbf{y}}';\tilde{\mathbf{a}}\right)=\frac{\left[\sum_{k=1}^{2}\sum_{i=1}^{N}w_k'\left(i\right)\frac{p'\left(y_k'\left(i\right);a_k\left(i\right),H_0\right)}{p\left(y_k'\left(i\right);a_k\left(i\right),H_0\right)}\right]^2}{\frac{1}{2N}\left[\sum_{k=1}^{2}\sum_{i=1}^{N}w_k'\left(i\right)\right]^2\left[\sum_{k=1}^{2}\sum_{i=1}^{N}\frac{p'\left(y_k'\left(i\right);a_k\left(i\right),H_0\right)}{p\left(y_k'\left(i\right);a_k\left(i\right),H_0\right)}\right]^2} \underset{H_0}{\overset{H_1}{\gtrless}} T \quad , \tag{17}$$

where $p'\left(y_k'\left(i\right);a_k\left(i\right),H_0\right)$ is the derivative of the pdf with respect to the observations [29]. It is noted that in Eq. (17) it is only the watermark shape $\mathbf{w}_k'$ (not the parameter γ) that is necessary for the Rao detector.

Substituting the pdfs model into Eq. (17), we obtain

$$T_R\left(\tilde{\mathbf{y}}';\hat{\tilde{\mathbf{a}}}_{/H_0}\right)=\frac{\left[\sum_{k=1}^{2}\sum_{i=1}^{N}w_k'(i)\,\hat{a}_{k/H_0}(i)\,y_k'(i)\right]^2}{\frac{1}{2N}\sum_{k=1}^{2}\sum_{i=1}^{N}\left(w_k'(i)\right)^2\sum_{k=1}^{2}\sum_{i=1}^{N}\left(\hat{a}_{k/H_0}(i)\,y_k'(i)\right)^2}\underset{H_0}{\overset{H_1}{\gtrless}}T \quad , \tag{18}$$

where $\hat{\tilde{\mathbf{a}}}_{/H_0}$ is the estimated value of $\tilde{\mathbf{a}}$ under hypothesis H_0.

Interestingly, the Rao detector assumes the form of a normalized correlation detector, where the watermark shape is correlated with the normalized observations. One may recall that earlier the *PGLRT* detector in its simplified form in Eq. (12) also assumes the form of a correlator. The Rao detector in Eq. (18) is invariant with respect to the strength of the watermark. The parameter estimates $\hat{a}_{k/H_0}(i)$ are also obtained by the MAP methodology as for the *PGLRT* detector in Eq. (13).

5. NUMERICAL EXPERIMENTS

Numerical experiments are used to test the performance of the detectors based on the proposed image model. At first four commonly used test images (of size 512×512, shown in *Figure 1*) in image processing tasks were used in our experiments to demonstrate our detectors. Then, in order to establish statistical significance of our results we used 200 representative images (10 from each one of the 20 categories) of the Microsoft Image Recognition data base [30]. These images were interpolated to size 512×512. In *Figure 2* we show a representative sample of 40 of these 200 images used.

To quantify the power of the watermark in our experiments, the so-called watermark to document ratio (WDR) is used, which is defined as

$$WDR=20\log_{10}\left(\frac{\|\gamma\mathbf{w}\|}{\|\mathbf{f}\|}\right)dB\,. \tag{22}$$

To quantify the detection performance, the receiver operating characteristics (ROC) curves are used. In particular, the area under the ROC (AUROC) curve for false alarm probability range [0-0.1] is used to quantify the performance of the detector at low false alarm

rates; the total area under the ROC curve is also computed to quantify the overall performance of the detector. These two metrics are referred to as AUROC1 and AUROC2, respectively, in the rest of the paper.

ROCs curves were obtained using two approaches:

i) A set of 100 different randomly generated 1-bit spread spectrum watermarks [1] were used for each image in *Figure 1* at a specified WDR. For each watermark the test statistic was evaluated twice, once with the watermarked and once with the un-watermarked image. The histograms of the test statistic for the two cases are then computed based on which the ROC curve is generated using a moving threshold. In other words, for this approach "random watermarks" were used to obtain ROCS for fixed images.

ii) The 200 images were added to the same watermark. Then, the test statistic was evaluated for the 200 images with the watermark and the 200 images without the watermark. Thus, histograms of the test statistic for the two cases were created from which ROC curves were generated. In other words, for this approach "random images" were used to obtain ROCs for fixed watermarks.

For comparison purposes we considered detectors that are based on wavelet transform and GGD modeling. These detectors represent the state-of-the-art methods for additive watermark detection. To the best of our knowledge, a non-adaptive wavelet model is typically used in the existing work in the literature, e.g., [5] and [7], where a single GGD model is assumed for all wavelet bands. In our experiments, we considered an "adaptive" wavelet GGD model, in which we used a different GGD model for each wavelet band. Our experiments demonstrate that an adaptive wavelet GGD model can lead to better detection performance than a non-adaptive model. Thus, we report our comparison results based on this adaptive wavelet GGD model. For completeness, we provide the detail of these wavelet GGD based detectors in the Appendix. Hereafter these detectors are referred to as wavelet GGD detectors.

For fairness to the wavelet GGD detectors, watermarking was performed in the wavelet domain of the images. The watermark was imbedded in the 2nd level of the discrete wavelet transform (DWT), as illustrated in *Figure 3*. The Daubechies-8 2-D separable filters were used [35]. In all experiments the watermarked images were first quantized using 8 bits per pixel accuracy in the spatial domain before watermark detection.

For the wavelet GGD detectors the watermark detection was performed directly in the wavelet domain using the watermarked coefficients. For our proposed detectors, the wavelet domain watermark was first transformed back to the spatial domain before the detection was performed.

For the proposed model the parameters m and l of the Gamma hyper-prior were determined as follows in our experiments. As mentioned earlier, as $l \to \infty$ we have from (13) $\hat{a}_k(i) = \frac{1}{2m}$, which corresponds to a stationary model. In such a model we can easily find the ML estimate of the residual variance as $\left(\hat{a}_{STAT}\right)^{-1} = \frac{1}{N}\|\boldsymbol{\varepsilon}\|^2$ with $\boldsymbol{\varepsilon} = \frac{1}{2}\left(\mathbf{Q}_1 + \mathbf{Q}_2\right)\mathbf{f}$, which is the "average" of the 2 IDDs. Then, the parameter m is estimated as $m = \frac{1}{2\hat{a}_{STAT}}$. The parameter l was selected empirically in such a way that the histogram of the resulting normalized IDDs $\varepsilon'_k(i) = \left(a_k(i)\right)^{\frac{1}{2}} \varepsilon_k(i)$, $k = 1,2$, and $i = 1,2 \ldots N$ would best fit a standard Gaussian pdf. The procedure in [20] and [21] was used to fit the histograms. The example mentioned earlier in Figure 4 was obtained using this procedure, where the estimated parameters $\hat{a}_k^{-1}(i)_{/H_0}$ were shown for the "Lena" image.

In what follows we present four experiments were we test the proposed detectors. In the first three averaging over random watermarks is used while in the last one averaging over images is used to test different detectors.

Experiment I: The simplified *PGLRT* detector in Eq. (12) was tested. The AUROC1 and AUROC2 metrics for this detector are summarized in *Tables 1(a)-(d)* for various WDR levels for the images in *Figures 1(a)-(d)*, respectively. For comparison, the results of the adaptive

wavelet domain *PGLRT* detector (in Eq. (A.2)) are also given. From these results we observe that the proposed *PGLRT* detector outperforms the wavelet GGD detector.

Experiment II: The Bayesian detector in Eq. (15) was compared with the *PGLRT* detector. The AUROC1 and AUROC2 of the Bayesian detector are summarized in *Tables 2(a)-(d)* for the same set of test images. Compared with the results *Tables 1(a)- (d)*, it can be seen that the performance of the Bayesian detector is inferior to that of the *PGLRT* detector; nevertheless, the overall performance of the Bayesian detector is close to that of the wavelet GGD detector. Among the four test images, the two methods were about the same in two images ("*Barbara*" and "*Lena*"), while the Bayesian detector was better in the "*Bridge*" image and worse in the "*Boat*" image. In *Figures 5(a)-(d)* we show some ROC curves obtained for the *PGLRT*, Bayesian, and wavelet GGD detectors.

Experiment III: The Rao test detector in Eq. (18) was tested. The AUROC1 and AUROC2 results are summarized in *Tables 3(a)-(d)* for the test images in *Figure 1*. For comparison, results are also furnished for the corresponding Rao test detector based on the "adaptive" wavelet GGD model in Eq. (A.3). In addition, we show in *Figures 6(a)-(d)* some ROC curves obtained for the two detectors. From these results, we observe that the proposed Rao test detector outperforms the wavelet GGD Rao test detector. Furthermore, by comparing with the earlier results in *Tables 1(a)-(d)*, we observe that the *PGLRT* detector outperforms the Rao test detector. This is not unexpected because the Rao test does not assume knowledge of the watermark power.

Experiment IV: In this experiment we tested all three proposed detectors for a number of WDRs using a set of 200 images and the same watermark as explained above. More, specifically, in *Tables 4(a)-(c)* we summarize AUROC1 and AUROC2 results for different WDRs for the GLRT detectors using both GGD wavelet, and the proposed prior, the Bayesian detector, and the Rao test using both GGD wavelet, and the proposed prior. In *Figure 7 (a)-(d)* we show the ROCs for the proposed detectors and the corresponding wavelet GGD based detectors. From the AUROC and the ROCs in these tables and figures the superiority of the detectors based on the proposed prior for this experiment is also clear. It is worth noting at

this point, for the sake of simplicity, the *same* value of the Gamma hyper prior parameter -*l*- was used for all test images. Thus, in this experiment the detectors based on the proposed prior have a handicap as compared to the previous experiments where these parameter was adapted to the statistics of each image as explained above. In spite of this, the proposed detectors worked out equally well in this experiment also.

To test the robustness of the proposed *PGLRT* detector JPEG compression attacks were used. Detection performance of our detector degraded gracefully as the quality factor decreased. In *Figures 8 (a), (b)* we show for two different images ("Lena", "Barbara"), the ROC curves for the *PGLRT* detector without and with JPEG compression attacks (quality 95% and 80%).

In *Figures 9 (a), (b)* also show the histograms of *PGLRT* test statistic. The first case is when one image and many different watermarks are used, while the second one is when the images from the database (200 images) and a common watermark are used, see ROC generation approaches (i) and (ii) explained previously.

Finally, as far as computational complexity concerned, for computing the test statistic for 200 images (100 with valid watermarks and 100 with invalid watermarks) it took approximately 20, 6, and 35 minutes, respectively, for the proposed *PGLRT*, Bayesian and Rao test detectors. For the wavelet GGD detectors, it took approximately 6.5 minutes and 6.2 minutes, respectively, for the *PGLRT* and Rao test. These detectors were implemented in Matlab on a Pentium-4 3.2 GHz PC. The above reported run time also includes the time needed for estimating the model parameters in each case.

6. CONCLUSIONS AND FUTURE WORK

In this paper we presented a new class of detectors based on a spatially adaptive image prior. This prior has the ability to explicitly model the local image discontinuities (edges) based on the variance parameters $a_k(i)$ of the local IDDs of the image. The derived detectors were demonstrated to show notable improvement over their counterparts derived from the

state-of-the-art wavelet based image models. Also, the *PGLRT* and Rao test detectors were demonstrated to achieve better performance than the Bayesian detector.

We note that, in addition to the results presented in the paper, we also tested these detectors with several other images, including JPEG compressed watermark images. In all these tests similar results were obtained to what were presented in the paper. These results were not included here in favor of space. As the results show, the proposed detectors are somewhat more computationally expensive than the wavelet GGD detectors, a trade-off with better detection performance.

The performance of the proposed detectors depends on the estimates of the parameters $a_k(i)$ and the hyper-prior parameters m and l. In this work we used a MAP approach to estimate $a_k(i)$ and an empirical method to estimate m and l. We expect that additional gains can be achieved if a Bayesian methodology is used to estimate these parameters. One possible direction might be to explore a simultaneous image segmentation and estimation of these parameters. Also another important issue that was not addressed in this work is determining the detection performance limits of the proposed scheme and how close we can get to them.

We believe that the fields of image recovery and watermark detection although seemingly very different share certain commonalities. More specifically, they both use statistical models to describe the unknown image. Thus, accurate and flexible models developed for one of these fields can be very beneficial to the other. In this paper we have just demonstrated this point.

APPENDIX: WAVELET GGD BASED DETECTORS

In wavelet based GGD models, the wavelet coefficients $X(i)$ of the image, where i denotes the spatial index of the wavelet coefficients, are modeled as IID GGD random variable with pdf given by

$$p(X(i)) = A\exp(-|bX(i)|^c), \tag{A.1}$$

where c is known as the shape parameter of the distribution, $b = \frac{1}{\sigma} n(c)$ and $A = \frac{bc}{2\Gamma(1/c)}$,

with $n(c) = \sqrt{\frac{\Gamma(3/c)}{\Gamma(1/c)}}$ and $\Gamma(t) = \int_0^\infty u^{t-1} e^{-u} du$. Here the unknown parameters are $\{c, b\}$. When the shape parameter $c_k = 2$, the GGD becomes the well known Gaussian.

In our comparison, we considered an "adaptive" GGD wavelet model, in which we used a different GGD model for each wavelet band. The test statistics for the GLRT and the Rao test detectors are given respectively by

$$T_{GLRT-GGD}(\mathbf{X};\mathbf{b},\mathbf{c}) = \sum_{k=1}^{K}\sum_{i_k=1}^{N_K} b_k^{\,c_k} \left(\left|X_k(i_k)\right|^{c_k} - \left|X_k(i_k) - W_k''(i_k)\right|^{c_k} \right), \tag{A.2}$$

and

$$T_{RAO-GGD}(\mathbf{X};\mathbf{c},\mathbf{b}) = \frac{\left[\sum_{k=1}^{K}\sum_{i_k=1}^{N_k} sign\left(X_k(i_k)\right)\left|X_k(i_k)\right|^{c_k-1} W_k'(i_k)\right]^2}{\frac{1}{\sum_{k=1}^{K} N_k}\left[\sum_{k=1}^{K}\sum_{i_k=1}^{N_k} W_k'(i_k)^2\right]\left[\sum_{k=1}^{K}\sum_{i_k=1}^{N_k}\left|X_k(i_k)\right|^{2(c-1)}\right]}, \tag{A.3}$$

where i_k denotes the i-th coefficient in the k-th band, N_k is the total number of coefficients in k-*th* band, and K is the number of bands. The vector $\mathbf{X} = \left[X_1(1)\ldots X_1(N_1)\ldots X_K(1)\ldots X_K(N_K)\right]$ includes all the wavelet coefficients of the image; $\left[W_1''(1)\ldots W_1''(N_1)\ldots W_K''(1)\ldots W_K''(N_K)\right]$ is the watermark when the watermark power is known; and $\left[W_1'(1)\ldots W_1'(N_1)\ldots W_K'(1)\ldots W_K'(N_K)\right]$ is the watermark shape. The vectors $\mathbf{b} = \left[b_1, b_2 \ldots b_K\right]$ and $\mathbf{c} = \left[c_1, c_2 \ldots c_K\right]$ denote the GGD model parameters in the K bands. The ML estimates of $\{c_k, b_k\}$ were used for the GLRT and Rao detectors, which were determined for each wavelet band separately.

In our experiments $K = 3$ and $N_k = \left(\frac{M}{4}\right)^2$ for $k = 1,2,3$ were used for original images of size $M \times M$.

REFERENCES

[1] I. Cox, M. Miller, and J. Bloom, *Digital Watermarking*, Morgan Kaufman, 2002.

[2] G. C. Langelaar, I. Setyawan, and R. L. Lagendijk, "Watermarking digital image and video data: A state-of-the-art overview," *IEEE Signal Processing Magazine*, vol. 17, no. 5, pp. 20-46, September 2000.

[3] J. R. Hernandez, M. Amado, and F. Perez-Gonzalez, "DCT-domain watermarking techniques for still images: Detector performance analysis and a new structure," *IEEE Trans. on Image Processing*, vol. 9, no. 1, pp. 55-68, Jan. 2000.

[4] M. Barni, F. Bartolini, A. D. Rosa and A. Piva, "Optimum decoding and detection of multiplicative watermarks," *IEEE Trans. on Signal Processing*, vol. 51, no. 4, April 2003.

[5] Q. Cheng and T. S. Huang, "An additive approach to transform-domain information hiding and optimum detection structure," *IEEE Trans. on Multimedia*, vol. 3, no. 3, Sept. 2001.

[6] Q. Cheng and T. S. Huang, "Robust optimum detection of transform domain multiplicative watermarks*," IEEE Trans. on Signal Processing*, vol. 51, no. 4, April 2003.

[7] A. Nikolaidis and I. Pitas, "Asymptotically optimal detection for additive watermarking in the DCT and DWT domains," *IEEE Trans. on Image Processing*, vol. 12, no. 5, pp. 563-571, May 2003.

[8] A. Briassouli, P. Tsakalides, and A. Stouraitis, "Hidden messages in heavy-tails: DCT-domain watermark detection using alpha-stable models," *IEEE Trans. on Multimedia*, Vol. 7, pp. 700-715, No. 4, August 2005.

[9] P. Maragos, R. Schafer, and R. Mersereau, "Two-dimensional linear prediction and its application to adaptive predictive coding of images," *IEEE Trans. on Acoustics, Speech, and Signal Processing*, vol. 32 no. 6, pp. 1213-1229, Dec 1984.

[10] G. Demoment, "Image restoration and reconstruction: overview of common estimation structures and problems," *IEEE Trans. on Acoustics Speech and Signal Processing*, vol. 37, pp. 2024-2036, December 1989.

[11] N. P. Galatsanos and A. K. Katsaggelos, "Methods for choosing the regularization parameter and estimating the noise variance in image restoration and their relation," *IEEE Trans. Image Processing*, vol. 1, pp. 322-336, July 1992.

[12] R. Molina, "On the hierarchical Bayesian approach to image restoration: applications to astronomical images," *IEEE Transactions on Pattern Analysis and Machine Intelligence*, vol. 16, no. 11, 1122-1128, November 1994.

[13] R. Molina, A. K. Katsaggelos, and J. Mateos, "Bayesian and regularization methods for hyper-parameter estimation in image restoration," *IEEE Trans. on Image Processing*, vol. 8, no. 2, pp. 231 -246, Feb. 1999.

[14] R. Molina, and B. D. Ripley, "Using spatial models as priors in astronomical images analysis," *Journal. Applied Statistics*, vol.16, pp.193-206, 1989.

[15] C. Bouman and K. Sauer, "A generalized Gaussian image model for edge-preserving MAP estimation," *IEEE Trans. on Image Processing*, vol. 2, no. 3, pp. 296-310, July 1993.

[16] M. A. T. Figueiredo and R. D. Nowak, "An EM algorithm for wavelet-based image restoration," *IEEE Trans. on Image Processing* , vol. 12, no. 8, pp. 866- 881, August 2003.

[17] M. Belge, M. Kilmer, and E. Miller, "Wavelet domain image restoration with adaptive edge preserving regularization," *IEEE Trans. on Image Processing*, vol. 9, no. 4, pp. 597-608, April 2000.

[18] S. Chang, Bin Yu, M, Vetterli, "Spatially adaptive wavelet thresholding with context modeling for image denoising," *IEEE Trans. on Image Processing*, vol. 9, no. 9, pp. 1522-1531, September. 2000.

[19] P. Moulin, J. Liu, "Analysis of multiresolution image denoising schemes using generalized Gaussian and complexity priors,", *IEEE Trans. on Information Theory*, vol. 45, no. 3, pp. 909 – 919, April 1999.

[20] M. N. Do and M. Vetterli, "Wavelet-based texture retrieval using generalized Gaussian density and Kullback-Leibler distance," *IEEE Trans. on Image Processing*, vol. 11, no. 2, pp. 146-158, Feb. 2002.

[21] M. Pi, "Improve maximum likelihood estimation for subband GGD parameters," *Pattern Recognition Letters*, 2006.

[22] G. Chantas, N. P. Galatsanos, and A. Likas, "Bayesian restoration using a new nonstationary edge preserving image prior", *IEEE Trans. on Image Processing*, Vol. 15, No. 10, pp. 2987-2997, October 2006.

[23] F-C. Jeng, J. W. Woods, "Compound Gauss-Markov fields for image estimation," *IEEE Trans. on Signal Proc*. vol. 39, no. 3, March 1991.

[24] R. Molina, A. K. Katsaggelos, Javier Mateos, A. Hermoso, C. Andrew Segall, "Restoration of severely blurred high range images using stochastic and deterministic relaxation algorithms in compound Gauss-Markov random fields," *Pattern Recognition* vol 33, pp. 555-571, 2000.

[25] M. E. Tipping "Sparse Bayesian learning and the relevance vector machine," *Journal of Machine Learning Research* 1, pp. 211-244, 2001.

[26] J. Berger, *Statistical Decision Theory and Bayesian Analysis*, Springer Verlag, 1985.

[27] N. Galatsanos, V. N. Mesarovic, R. M. Molina, J. Mateos, and A. K. Katsaggelos, "Hyper-parameter estimation using gamma hyper-priors in image restoration from partially-known blurs," *Optical Engineering*, 41(8), pp. 1845-1854, August 2002.

[28] S. M. Kay, *Fundamental of Statistical Signal Processing: Detection Theory*, vol. 2 Prentice Hall, 1998.

[29] S. M. Kay, "Asymptotically optimal detection in incompletely characterized non-Gaussian noise," *IEEE Trans. Acoust., Speech, Signal Processing*, vol. 37, no. 5, pp. 627–633, May 1989.

[30] Microsoft Research Cambridge Object Recognition Image Database http://research.microsoft.com/downloads

[31] C. M. Bishop, *Pattern Recognition and Machine Learning*, Springer 2006.

[32] S. Roth, M. J. Black, "Fields of Experts: A Framework for Learning Image Priors", *IEEE Conf. on Computer Vision and Pattern Recognition*, vol. II, pp. 860-867, June 2005.

[33] D. Tzikas, A. Likas and N. Galatsanos, "Variational Bayesian Blind Image Deconvolution with Student-T Priors", *IEEE International Conference on Image Processing*, San Antonio Texas, 2007.

[34] J. Chantas, N. P. Galatsanos, and N. Woods, "Super Resolution Based on Fast Registration and Maximum A Posteriori Reconstruction", *IEEE Trans. on Image Processing*, Vol. 16, No. 7, pp. 1821-1830, July 2007.

[35] I. Daubechies. Orthonormal bases of compactly supported wavelets. Commun. On Pure and Appl. Math., 41:909-996, November 1988

(a) "Barbara"

(b) "Boat"

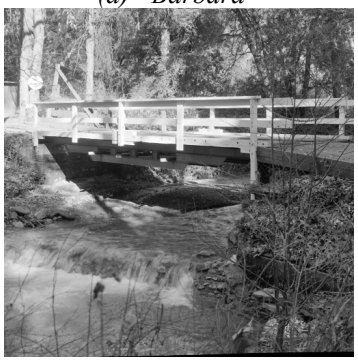

(c) "Bridge"

(d) "Lena"

Figure 1(a)-(d): The four test images used to evaluate the proposed detectors in *Experiments I-III*.

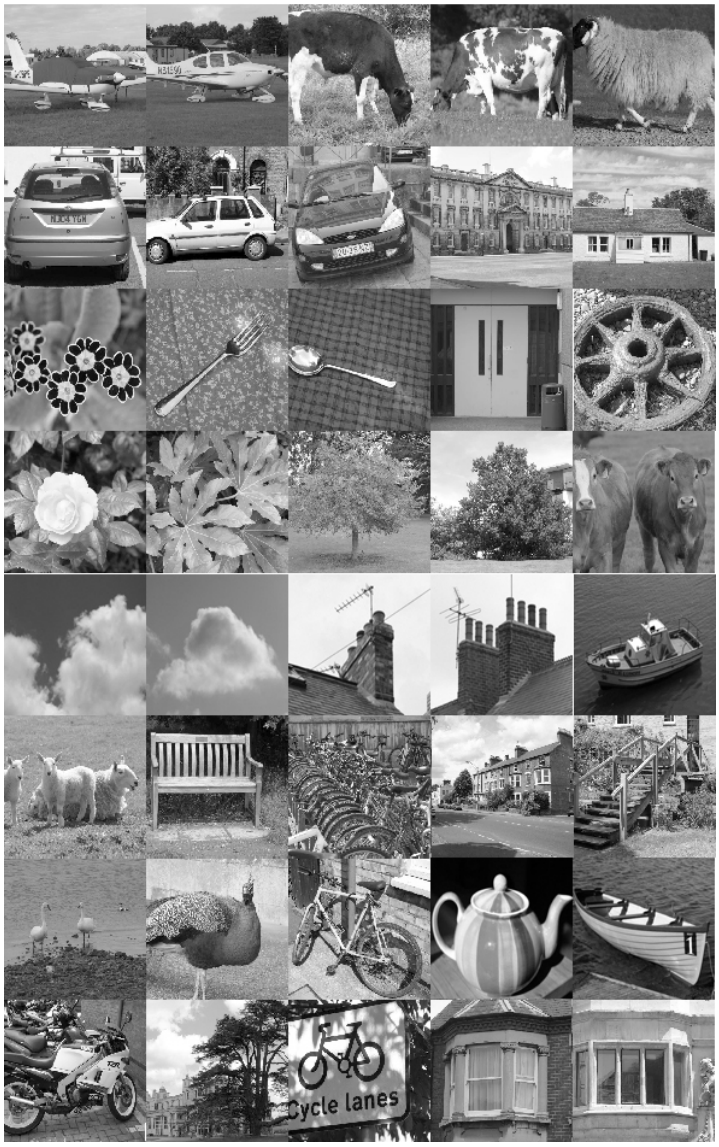

Figure 2: A sample of 40 of the 200 images used to evaluate the proposed detectors in *Experiment IV*.

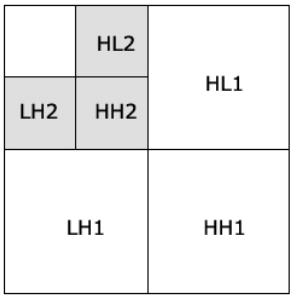

Figure 3: Watermark embedding in the three detail sub-bands of the second level of a 2-level DWT was used.

(a) (b)

Figure 4: Values of $\log\left(a_k^{-1}(i)\right)$ for the 1st order differences along: (a) horizontal, and (b) vertical directions.

WDR dB	***(AUROC1, AUROC2)***	
	GGD Wavelet	***Proposed Prior***
-61	(0.100, 1.000)	(0.100, 1.000)
-62	(0.0991, 0.99)	(0.100, 1.000)
-63	(0.0593, 0.92)	(0.100, 1.000)
-64	(0.0133, 0.64)	(0.0940, 0.993)
-65	(0.0060, 0.52)	(0.0903, 0.986)
-66	(0.0034, 0.50)	(0.0848, 0.981)

(a)

WDR dB	***(AUROC1, AUROC2)***	
	GGD Wavelet	***Proposed Prior***
-64	(0.100, 1.00)	(0.0993, 0.9993)
-65	(0.0095, 0.90)	(0.0922, 0.9894)
-66	(0.004, 0.62)	(0.0892, 0.9784)
-67	(0.004, 0.50)	(0.0769, 0.9489)

(b)

Tables 1(a)-(b): AUROC1 and AUROC2 for the *PGLRT* detector with: (a) "*Barbara*", (b) "*Boat*" images.

WDR dB	***(AUROC1,AUROC2)***	
	GGD Wavelet	***Proposed Prior***
-60	(0.100, 1.000)	(0.100, 1.000)
-61	(0.0979, 0.99)	(0.100, 1.000)
-62	(0.0706, 0.94)	(0.100, 1.000)
-63	(0.0302, 0.75)	(0.0942, 0.993)
-64	(0.0087, 0.58)	(0.0697, 0.946)
-65	(0.0057, 0.51)	(0.0624, 0.880)

(c)

WDR dB	***(AUROC1,AUROC2)***	
	GGD Wavelet	***Proposed Prior***
-62	(0.100, 1.000)	(0.100, 1.000)
-63	(0.0965, 0.99)	(0.100, 1.000)
-64	(0.0279, 0.81)	(0.100, 1.000)
-65	(0.0092, 0.58)	(0.0991, 0.9991)
-66	(0.0056, 0.50)	(0.0987, 0.9987)

(d)

Table 1(c)-(d): AUROC results *PGLRT* detector with: (c) "*Bridge*" and (d) "*Lena*" images.

WDR dB	*(AUROC1, AUROC2)* *Bayesian detector*
-61	(0.100, 1.000)
-62	(0.0980, 0.998)
-63	(0.0512, 0.8748)
-64	(0.0110, 0.610)
-65	(0.0059, 0.5214)
-66	(0.0055, 0.5028)

(a)

WDR dB	*(AUROC1, AUROC2)* *Bayesian detector*
-64	(0.0366, 0.901)
-65	(0.0105, 0.61)
-66	(0.0058, 0.52)
-67	(0.0054, 0.503)

(b)

Table 2(a)-(b): AUROCs results of Bayesian detector with: (a) "*Barbara*", (b) "*Boat*" images.

WDR dB	*AUROC1, AUROC2* *Bayesian detector*
-60	(0.100, 1.000)
-61	(0.100, 1.000)
-62	(0.0809, 0.962)
-63	(0.0330, 0.757)
-64	(0.0093, 0.581)
-65	(0.0062, 0.524)

(c)

WDR dB	*AUROC1, AUROC2* *Bayesian detector*
-62	(0.100, 1.000)
-63	(0.100, 1.000)
-64	(0.0521, 0.898)
-65	(0.0082, 0.585)
-66	(0.047, 0.51)

(d)

Table 2(c)-(d): AUROC results of Bayesian detector with: (a) "*Bridge*", (b) "*Lena*" images.

WDR dB	*(AUROC1, AUROC2)*	
	Rao GGD Wavelet	*Rao Proposed Prior*
-59	(0.100, 1.000)	(0.100, 1.000)
-60	(0.0901, 0.97)	(0.100, 1.000)
-61	(0.0827, 0.96)	(0.100, 1.000)
-62	(0.0294, 0.76)	(0.100, 1.000)
-63	(0.0112, 0.68)	(0.0764, 0.9739)
-64	(0.0029, 0.51)	(0.0567, 0.8862)

(a)

WDR dB	*(AUROC1, AUROC2)*	
	Rao GGD Wavelet	*Rao Proposed Prior*
-61	(0.100, 1.000)	(0.100, 1.000)
-62	(0.0973, 0.98)	(0.100, 1.000)
-63	(0.0736, 0.94)	(0.100, 1.000)
-64	(0.0274, 0.66)	(0.0748, 0.983)
-65	(0.0217, 0.7163)	(0.0425, 0.830)
-66	(0.011, 0.6401)	(0.0213, 0.697)

(b)

Tables 3(a)-(b): Rao detectors AUROC results with: (a) "*Barbara*", (b) "*Boat*" images.

WDR dB	***(AUROC1, AUROC2)***	
	Rao GGD Wavelets	**Rao Proposed Prior**
-60	(0.100, 1.000)	(0.100, 1.000)
-61	(0.0827, 0.97)	(0.100, 1.000)
-62	(0.0355, 0.80)	(0.0982, 0.9982)
-63	(0.0100, 0.50)	(0.0709, 09315)

(c)

WDR dB	***(AUROC1, AUROC2)***	
	Rao GGD Wavelet	**Rao Proposed Prior**
-61	(0.100, 1.000)	(0.100, 1.000)
-62	(0.0851, 0.85)	(0.100, 1.000)
-63	(0.0366, 0.77)	(0.100, 1.000)
-64	(0.0083, 0.54)	(0.0847, 0.9929)
-65	(0.0051, 0.50)	(0.0568, 0.9037)

(d)

Tables 3(c)-(d): Rao detectors AUROC results with: (a) "*Bridge*", (b) "*Lena*" images.

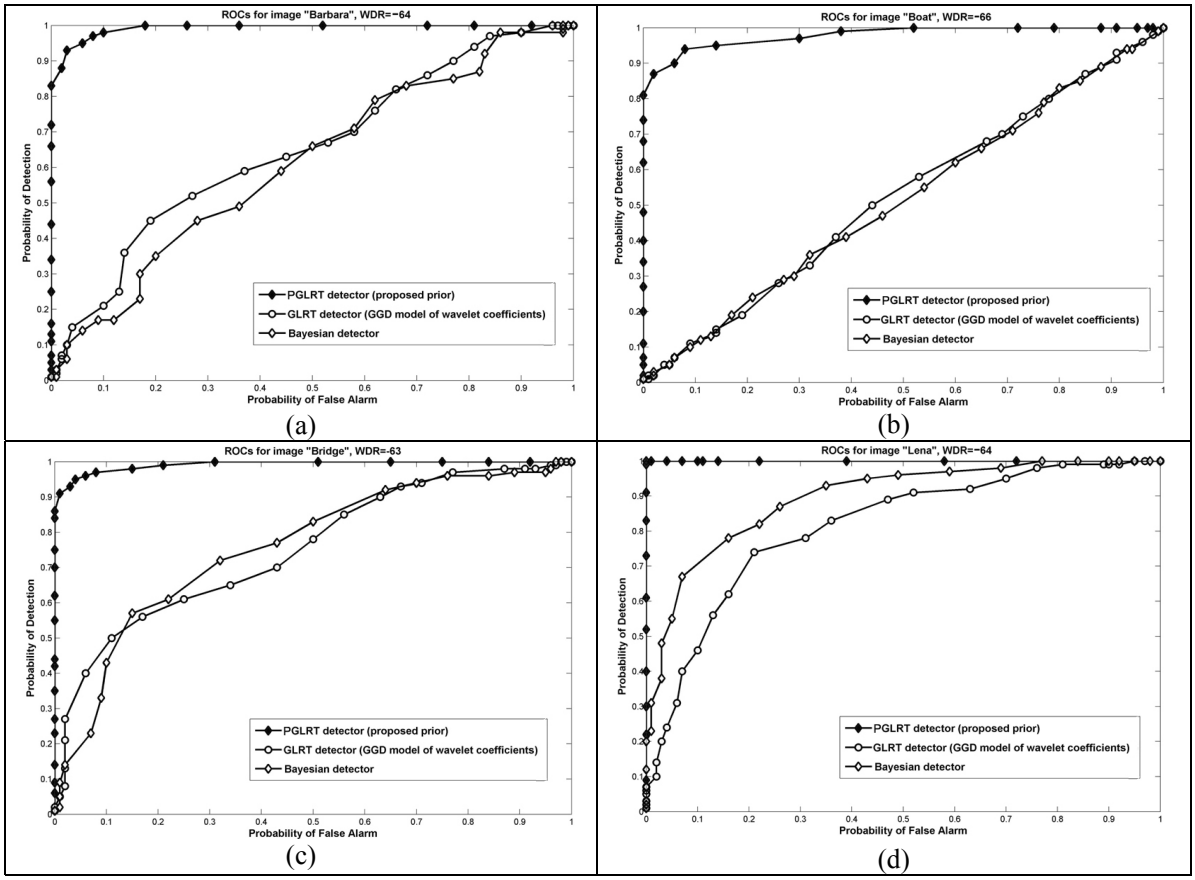

Figures 5(a)-(d): ROC curves of *PGLRT* and Bayesian detectors for selected *WDRs*

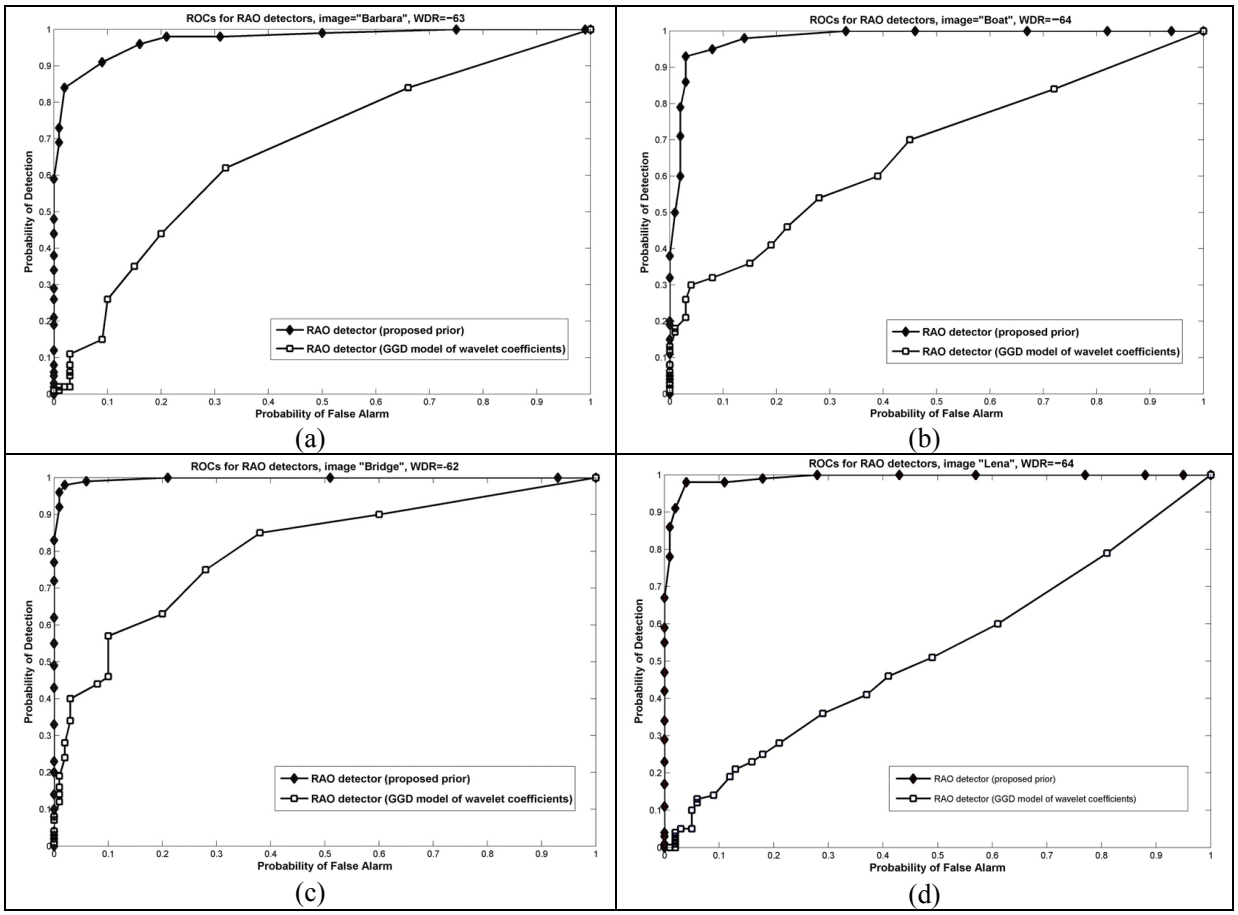

Figures 6(a)-(d): ROC curves of Rao test detectors for selected *WDRs*

WDR dB	***(AUROC1, AUROC2) GGD Wavelet***	***(AUROC1, AUROC2) PGLRT (proposed Prior)***
-61	(0.0540, 0.9925)	(0.0862, 0.9680)
-62	(0.0166, 0.7048)	(0.0785, 0.9540)
-63	(0.0041, 0.6039	(0.0831, 0.9512)
-64	(0.0052, 0.5307)	(0.0763, 0.9238)
-65	(0.0014, 0.5051)	(0.0746, 0.9149)

Tables 4(a):AUROC results for *PGLRT* detectors using 200 images.

WDR dB	***(AUROC1, AUROC2) BAYESIAN (proposed prior)***
-61	(0.0970, 0.9979)
-62	(0.0383, 0.8743)
-63	(0.0120, 0.6645)
-64	(0.0070, 0.5540)
-65	(0.0055, 0.5167)

Tables 4(b):AUROC results for Bayesian detector using 200 images.

WDR	*(AUROC1, AUROC2)*	*(AUROC1, AUROC2)*
	RAO GGD Wavelet	*RAO (proposed prior)*
-60	(0.0894, 0.9844)	(0.0993, 0.9992)
-61	(0.0675, 0.9679)	(0.0883, 0.9983)
-62	(0.0672, 0.9165)	(0.0775, 0.9848)
-63	(0.0348, 0.8001)	(0.0694, 0.9432)
-64	(0.0300, 0.5419)	(0.0389, 0.8106)

Tables 4(c):AUROC results for Rao test detectors using 200 images.

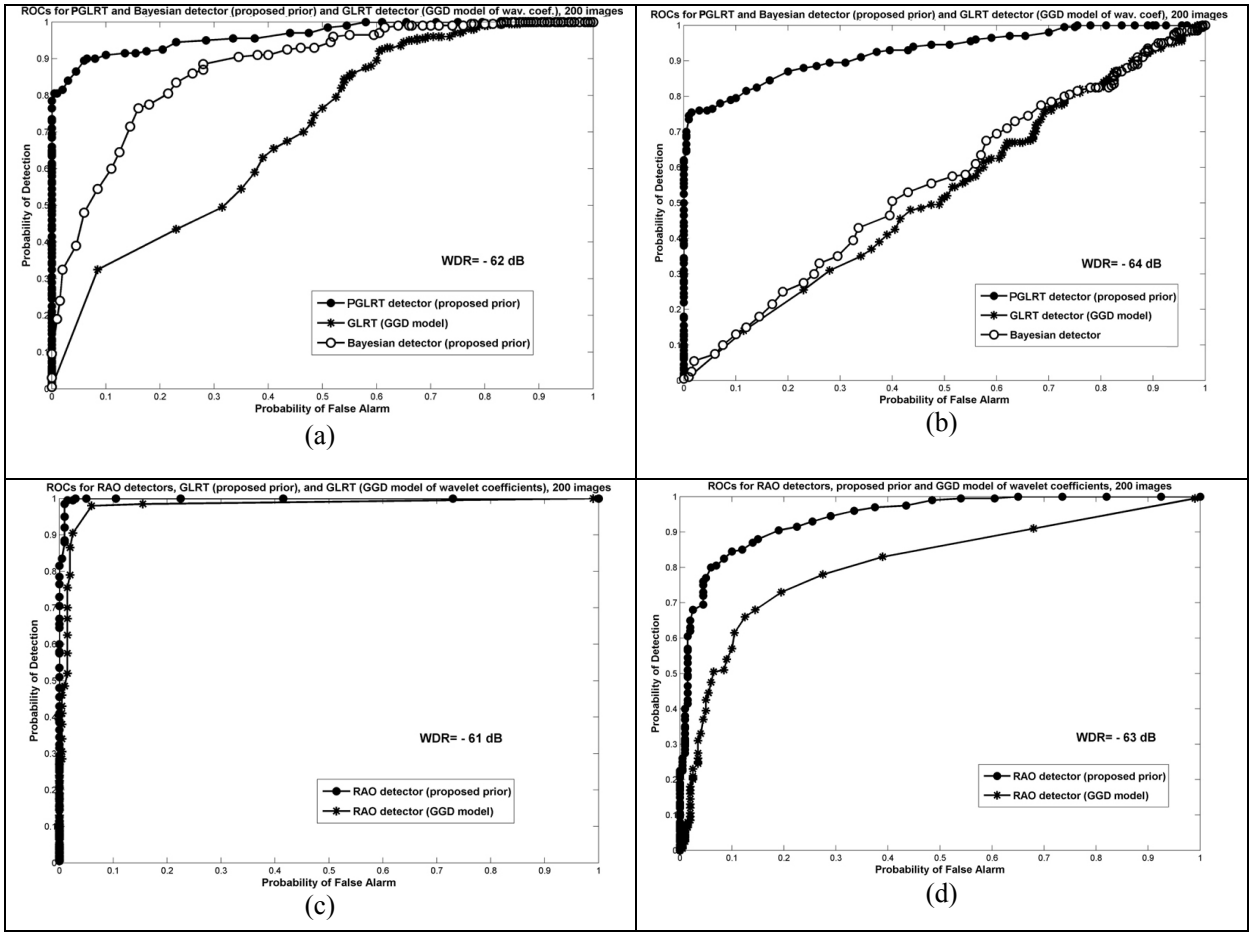

Figure 7: *(a), (b)* ROC curves for *PGLRT* and Bayesian detectors, *(c), (d)* ROC curves for Rao test based detectors, using 200 images.

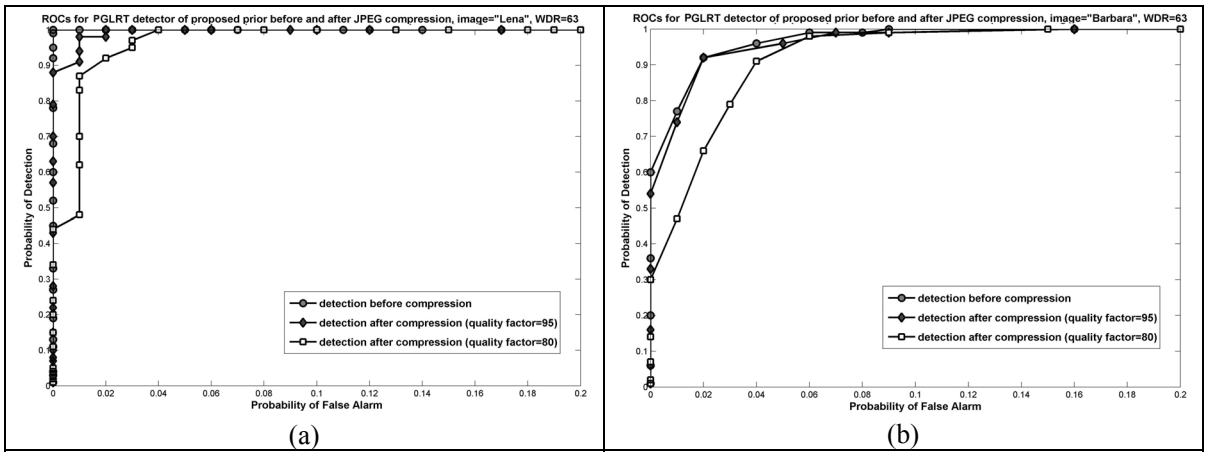

(a) (b)

Figure 8: ROC curves for *PGLRT* detector before and after JPEG compression (quality factor 95% and 80%) for *(a)* "Lena" and *(b)* "Barbara" images.

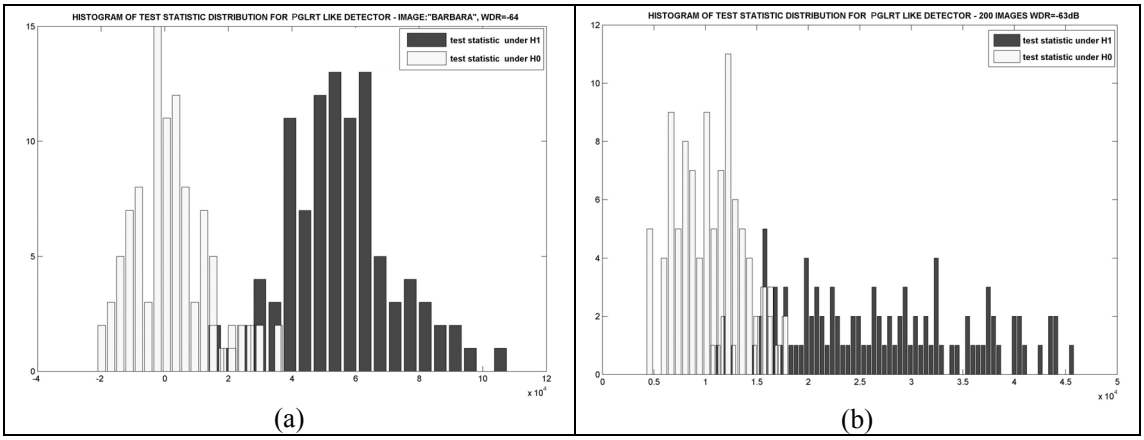

(a) (b)

Figure 9: Histogram of test statistic for *PGLRT* detector. *(a)* For one image and many watermarks, *(b)* for many images and one watermark.